Korea-Australia Rheology Journal (2023) 35:307–321
https://doi.org/10.1007/s13367-023-00070-1

ORIGINAL ARTICLE

The competing role of shear and extension-induced first normal stress differences within a mixed flow for a viscoelastic fluid

Huan-Chang Tseng[1,2]

Received: 23 May 2023 / Revised: 9 August 2023 / Accepted: 28 August 2023 / Published online: 12 September 2023

Abstract
Interested in the previous work of Walters et al. (Korea Aust Rheol J 21:225–233, 2009) regarding the competing roles of extensional viscosity and normal stress differences in complex flows of elastic liquids, rheological studies rarely discuss the relationship between the shear and extension-induced first normal stress differences (N1S and N1E) within a mixed flow for a viscoelastic fluid. One, therefore, derives N1S and N1E related to Weissenberg's number and Trouton's ratio. The classic White–Metzner viscoelastic constitutive equation coupled with the recent GNF-X (Generalized Newtonian Fluid eXtended) weighted shear/extension viscosity has the potential to show the typical vortex growth in entry flow simulations. Based on the improved White–Metzner model, demonstrating the opposite effect of N1S and N1E with respect to strain rates is evident. N1S mainly dominates the shell layer near the wall boundary at high strain rates, whereas N1E controls the center core at low strain rates. In contraction flow simulations, the predicted slit-die velocity profile is in good agreement with experimental data. It is significant to conclude that N1E hinders flow and N1S facilitates flow. In addition, a comparison of extensional-thickening and extensional-thinning viscosity curves for the velocity profile is discussed herein.

Keywords First normal stress difference · Shear flow · Extensional viscosity · Weissenberg's number · Trouton's ratio

1 Introduction

In rheology, viscoelasticity is the property of materials that exhibit both viscous and elastic characteristics when undergoing deformation. Generally, the elastic effect is related to the shear-induced first normal stress difference (N1S), $N_1^S = \tau_{11} - \tau_{22}$, wherein τ_{11} and τ_{22} denote the normal stresses in the principal flow and gradient directions, respectively. For a particular point of interest, extensional viscosity η_E is the ratio of "net tensile stress", $\sigma_E = \tau'_{11} - \tau'_{22}$, to extension rate $\dot{\varepsilon}$, namely, $\eta_E = \sigma_E/\dot{\varepsilon}$, wherein τ'_{11} and τ'_{22} denote the normal stresses in the principal stretch and shrink directions, respectively. Thus, σ_E is defined as the extensional-viscosity generating first normal stress difference (N1E), N_1^E. However, it is not normal to discuss the competitive role of N1S and N1E coexisting in complex flows for viscoelastic fluids of polymer melts.

Early on, Debbaut and Crochet [1] considered the effect of extensional viscosity as a cause of corner vortex in abrupt 4:1 contraction flow simulations. In addition, they concluded the conflicting effects of the extensional viscosity and N_1^S on vortex activity. Later, Walters et al. [2] used the Oldroyd B viscoelastic constitutive model to show the potential importance of N_1^S in axisymmetric contraction flows for Boger fluids. Specifically, they summarized that high η_E can retard the flow, whereas high N_1^S can have the opposite effect. James [3] investigated the possible role of shear-generated normal stresses to be extensional in nature. For Boger fluids flowing through arrays of rods, the increased flow resistance is related to the elasticity property N_1^S, and not to the extensional viscosity stress N_1^E. Although N_1^S is small, it cannot be ignored. However, their numerical results did not evidently demonstrate the opposite effect of N_1^S and N_1^E in those articles aforementioned.

In the rheology, the Deborah number De and Weissenberg number Wi are key dimensionless number to indicate the viscoelastic character of polymer melts [4]. Experimentally, De

✉ Huan-Chang Tseng
ivortseng@moldex3d.com

[1] CoreTech System (Moldex3D) Co., Ltd, ChuPei City, Hsinchu 30265, Taiwan

[2] Tai Yuen Hi-Tech Industrial Park, 8F-2, No. 32, Taiyuan St., Chupei City, Hsinchu County 302, Taiwan

is defined as the ratio of the characteristic time of the fluid λ to the characteristic time of the flow t_f:

$$\mathrm{De} = \lambda / t_f \tag{1}$$

Theoretically, Wi is the product of the shear rate $\dot{\gamma}$ and relaxation time λ:

$$\mathrm{Wi} = \lambda \dot{\gamma}. \tag{2}$$

At a large Weissenberg number or Deborah number, Wi >> 1 or De >> 1, the fluid will respond with elastic behavior like that of a solid. For Wi << 1 or De << 1, a liquid-like viscous state is expected, while there is sufficient time to relax during deformation. Wi ≈ 1 or De ≈ 1 implies the viscoelastic fluid. Addiontally, Pipkin diagram [5] is the relationship between De and Wi to represent different flow regimes of a material regarding viscometric flows, linear viscoelasticity, and nonlinear viscoelasticity.

Recently, Tseng [6] derived a potential weighted shear/extensional viscosity, called the GNF-X (Generalized Newtonian Fluid eXtended) model. For the 3D (three-dimensional) entry flow simulation of a low-density polyethylene (LDPE) melt, he [6], therefore, demonstrated the vortex formation in terms of the weighted viscosity and extensional flow. The earlier White–Metzner (WM) constitutive equation [7] expresses a relatively simple nonlinear viscoelastic fluid. Based on the GNF-X model, Tseng continued to develop a modification of the WM constitutive equation, called the WMT-X (WM eXtended by Tseng) model [8–10]. Such a model can pretty well fit the first normal stress difference for characterizing a fluid's elasticity, as well as its shear viscosity and extensional viscosity. The predicted vortex sizes are in good agreement with the experimental data. In the WMT-X numerical calculation carried out over a wide range of Deborah numbers, it is stably convergent.

Using the WMT-X viscoelastic fluid model, the primary objective of the present study is, therefore, to demonstrate the competitive role of shear and extension-induced first normal stress differences coexisting in complex flows of polymer melts. Additionally, one can derive N_1^S and N_1^E related to Weissenberg's number and Trouton's ratio. In contraction flow simulations, the numerical predictions of slit-die velocity profile at different viscous and viscoelastic constitutive equations, including GNF, GNF-X, and WMT-X, are compared with related experimental data. The governing equations and constitutive equations of polymer melts are introduced in the next section for completeness.

2 Theoretical background

The actual flow of polymer melts is complicated. In non-Newtonian fluid mechanics, the polymer processing is highly nonlinear, as the material properties are dependent upon flow and temperature conditions. For completeness, the governing equations of fluid dynamics, including those on continuity, motion, and energy, are addressed:

$$\frac{\partial \rho}{\partial t} + \nabla \cdot \rho \mathbf{v} = 0 \tag{3}$$

$$\frac{\partial}{\partial t}(\rho \mathbf{v}) + \nabla \cdot (\rho \mathbf{v}\mathbf{v}) = -\nabla P + \nabla \cdot \boldsymbol{\tau} + \rho \mathbf{g} \tag{4}$$

$$\rho C_P \left(\frac{\partial T}{\partial t} + \mathbf{v} \cdot \nabla T \right) = \nabla \cdot (k \nabla T) + \boldsymbol{\tau} : \mathbf{D}, \tag{5}$$

where ρ is the density; $\mathbf{v}$ is the velocity vector; t is the time; P is the pressure; $\boldsymbol{\tau}$ is the extra stress tensor; $\mathbf{g}$ is the acceleration vector of gravity; C_p is the specific heat; T is the temperature; k is the thermal conductivity. Note that the velocity gradient tensor $\nabla \mathbf{v}$, rate-of-deformation tensor $\mathbf{D}$, and vorticity tensor $\mathbf{W}$ are kinematic tensors; their relationships are expressed as follows:

$$\mathbf{D} = \frac{\nabla \mathbf{v} + (\nabla \mathbf{v})^T}{2} \tag{6}$$

$$\mathbf{W} = \frac{\nabla \mathbf{v} - (\nabla \mathbf{v})^T}{2}, \tag{7}$$

where $\mathbf{D}$ and $\mathbf{W}$ are the symmetric and anti-symmetric parts of $\nabla \mathbf{v}$, respectively.

For different viscous and viscoelastic fluids, a rheological state expression of the stress tensor $\boldsymbol{\tau}$ in terms of various kinematic tensors is called the so-called constitutive equation. The constitutive equations of interest, including the standard GNF (generalized Newtonian fluid) viscous model of shear viscosity, the extended GNF (GNF-X) viscous model of weighted shear/extensional viscosity, and the improved White–Metzner viscoelastic model of WMT-X (White–Metzner eXtended by Tseng), are introduced in the present study.

2.1 GNF shear and extensional viscosity

The famous GNF (generalized Newtonian fluid) shear viscosity model [4, 11–13] describes the mathematical relationship

between the tensors $\boldsymbol{\tau}$ and $\mathbf{D}$ in a steady-state, homogenous, and generalized 3D deformation, as follows:

$$\boldsymbol{\tau} = 2\eta_S(\dot{\gamma})\mathbf{D}, \tag{8}$$

where shear viscosity η_S, which is a nonlinear function of strain rate, indicates flow resistance in simple shear; the strain rate $\dot{\gamma}$ is the magnitude of the rate-of-deformation tensor, namely, $\mathbf{D}$: $\dot{\gamma} = \sqrt{2\mathbf{D} : \mathbf{D}}$.

The flow curves of shear viscosity dominate the flow behaviors of a variety of materials. Commonly, the Carreau model [12], a type of the GNF shear viscosity model, is often used to fit experimental viscosity data:

$$\eta_S(\dot{\gamma}) = \frac{\eta_0}{[1 + (\lambda\dot{\gamma})^2]^{\frac{1-n}{2}}}, \tag{9}$$

where λ is the characteristic time; n is the power index; η_0 is the Newtonian fluid (NF) constant viscosity or the zero-shear-rate viscosity. When $\dot{\gamma} = 0$, the GNF viscosity returns to the NF viscosity.

In rheology, the Trouton ratio Tr is the uniaxial extensional viscosity η_{UE} over shear viscosity η_S [13–15]:

$$\mathrm{Tr} = \frac{\eta_{UE}}{\eta_S}. \tag{10}$$

For the isotropic Newtonian viscosity [14], the Trouton ratio ideally equals 3, namely, Tr = 3. In particular, Tseng [6] proposed the Trouton ratio function for an interrelationship between nonlinear shear viscosity and nonlinear extensional viscosity,

$$\eta_{UE}(\dot{\gamma}) = \eta_S(\dot{\gamma})\mathrm{Tr}(\dot{\gamma}) \tag{11}$$

$$\mathrm{Tr}(\dot{\gamma}) = 3 + \frac{\mathrm{Tr}_0}{\left[1 + (\lambda_T\dot{\gamma})^{-2}\right]^{n_T}}, \tag{12}$$

where three parameters:Tr_0, λ_T, and n_T are the anisotropic factor, characteristic time, and power index, respectively. Equation (12) is an empirical equation fitted by the experimental extension viscosity data to describe the significant extension thinning and extension thickening characteristics,, refer to the previous work of Sarkar and Gupta [15]. Note the maximum value of $\mathrm{Tr}(\dot{\gamma})$ at large $\dot{\gamma}$, namely, max$\mathrm{Tr} = 3 + \mathrm{Tr}_0$.

2.2 GNF-X weighted shear/extensional viscosity

Recently, Tseng [6] derived the weighted shear/extensional viscosity $\eta_W(\dot{\gamma})$, called the eXtended GNF (GNF-X) model, as expressed below:

$$\boldsymbol{\tau} = 2\eta_W\mathbf{D} \tag{13}$$

$$\eta_W = (1 - W)\eta_S + W\eta_E \tag{14}$$

$$1 - W = \frac{\dot{\gamma}_S^2}{\dot{\gamma}^2} \tag{15}$$

$$W = \frac{\dot{\gamma}_E^2}{\dot{\gamma}^2} \tag{16}$$

$$\dot{\gamma}^2 = \dot{\gamma}_S^2 + \dot{\gamma}_E^2, \tag{17}$$

where W is the weighting function, also known as the extension fraction; η_S and η_E are the generalized shear and extensional viscosities with respect to strain rates, respectively.

$\dot{\gamma}_S$ and $\dot{\gamma}_E$ are characteristic shear and extensional rates, respectively. Note that the weighted function W represents the percentage of extension rate. When $W = 0$, the GNF-X weighted viscosity returns to the GNF shear viscosity. For the flow classification, $W = 0$ and $W = 1$ indicate viscometric (or shear) and extensional (or shearfree) flows, respectively. Notably, it cannot be used to identify a rigid body rotation. Details of the GNF-X weighted viscosity are available elsewhere [6].

However, Park [16] commented the GNF-X model in which those so-called principal shear and extension rates cannot represent the shear and extension rates correctly. Therefore, Tseng [17] have sufficiently demonstrated that the GNF-X numerical algorithm can decompose exact shear and extension rates validated in the analytical center-gated disk flow. Significantly, Wen et al. [18] performed the non-isothermal GNF-X flow simulations to estimate the extensional viscosity for various polymer melts.

Basically, the GNF-X weighted viscosity is similar to the early Schunk-Scriven experiential model of a linear combination (or arithmetic mean) of the two type-Carreau-type shear and extension viscosities [19]. Differently, the Schunk-Scriven weighting function depends on the Astarita flow-classification parameter [20], which is the related to the trace of the relative vorticity and rate-of-deformation tensors. Another alternative to employ, Scriven and coworkers [21] proposed the weighted geometric-mean viscosity. The concept of the mixed viscosity was previously explored in several articles [22–25].

Additionally, the uniaxial extensional flow is defined as follows:

$$\eta_{UE} = \frac{\tau_{11} - \tau_{22}}{\dot{\varepsilon}} \tag{18}$$

$$\boldsymbol{\tau} = \begin{bmatrix} \tau_{11} & 0 & 0 \\ 0 & \tau_{22} & 0 \\ 0 & 0 & \tau_{33} \end{bmatrix} \tag{19}$$

$$\mathbf{D} = \dot{\varepsilon} \begin{bmatrix} 1 & 0 & 0 \\ 0 & -\frac{1}{2} & 0 \\ 0 & 0 & -\frac{1}{2} \end{bmatrix}, \tag{20}$$

where τ_{11}, τ_{22}, and τ_{33} are the x-axial, y-axial, and z-axial normal stress tensor components, respectively; $\dot{\varepsilon}$ is an extension rate. Therefore, the generalized extensional viscosity η_E is related to the uniaxial extensional (UE) viscosity η_{UE},

$$\eta_E = \frac{\eta_{UE}}{3} = \frac{\tau_{11} - \tau_{22}}{3\dot{\varepsilon}}. \tag{21}$$

Such an extensional viscosity η_E is also known as the *stressing viscosity* of Meissner et al. [11, 26]. For planar extension, the stressing viscosity equals

$$\eta_E = \frac{\eta_{PE}}{4}. \tag{22}$$

In previous article of Tseng [6], the key part of Eq. (21) is not discussed for the GNF-X model in relating η_E and η_{UE}. The two most commonly used techniques for measuring extensional viscosity of polymer melts are the rheometric scientific RME (rheometric melt elongation) rheometer and the Münstedt tensile rheometer [27]. In practice, it is difficult to directly measure the steady extensional viscosity of thermoplastic composite materials at high extension rates. The Cogswell analytic method of extensional viscosity was famously derived in the pressure drop of entrance flow for capillary rheometer [28].

2.3 WMT-X viscoelastic constitutive equation

Based on the GNF-X weighed shear/extension viscosity [6], Tseng [8] improved the classic White–Metzner (WM) viscoelastic constitutive equation, named WMT-X (WM eXtended by Tseng):

$$\lambda_W(\dot{\gamma})\overset{\square}{\boldsymbol{\tau}} + \boldsymbol{\tau} = 2\eta_W(\dot{\gamma})\mathbf{D} \tag{23}$$

where $\lambda_W(\dot{\gamma})$ is Weissenberg's relaxation time; $\overset{\square}{\boldsymbol{\tau}}$ is the Gordon–Schowalter time derivative [12]. Its complete form is expanded as follows:

$$\lambda_W(\dot{\gamma})\frac{\partial \boldsymbol{\tau}}{\partial t} + W_i(\dot{\gamma})\left(\frac{\mathbf{v}}{\dot{\gamma}} \cdot \nabla\boldsymbol{\tau}\right) - Wi(\dot{\gamma})[(\mathbf{W}^* \cdot \boldsymbol{\tau} + \boldsymbol{\tau} \cdot \mathbf{W}^{*T}) + C_N(\dot{\gamma})(\mathbf{D}^* \cdot \boldsymbol{\tau} + \boldsymbol{\tau} \cdot \mathbf{D}^*)] + \boldsymbol{\tau} = 2\eta_W(\dot{\gamma})\mathbf{D} \tag{24}$$

$$C_N(\dot{\gamma}) = 1 - \xi(\dot{\gamma}) \tag{25}$$

$$\mathbf{D}^* = \mathbf{D}/\dot{\gamma} \tag{26}$$

$$\mathbf{W}^* = \mathbf{W}/\dot{\gamma}, \tag{27}$$

where Wi is Weissenberg's number; $\mathbf{D}^*$ and $\mathbf{W}^*$ are dimensionless tensors of the rate-of-deformation tensor $\mathbf{D}$ and the vorticity tensor $\mathbf{W}$, respectively; the variable $C_N(\dot{\gamma})$ is the normal stress parameter limited between 0 and 1; the variable $\xi(\dot{\gamma})$ is a slip factor. When $\eta_W = \eta_S$, the WMT-X model returns to the White–Metzner model. Note that $\xi = 0$ and 1 signify the upper-convected and corotational forms, respectively. For a constant viscosity and $\xi = 0$, WMT-X is equivalent to UCM (upper convected Maxwell).

Especially for the "steady-state" and "homogenous" flows, the WMT-X stress tensor can be simplified to consist of the viscous and elastic terms:

$$\boldsymbol{\tau} = \underbrace{2\eta_W\mathbf{D}}_{\text{viscous}} + \underbrace{\text{Wi}[(\boldsymbol{\tau} \cdot \mathbf{W}^* + \mathbf{W}^{*T} \cdot \boldsymbol{\tau}) + C_N(\boldsymbol{\tau} \cdot \mathbf{D}^* + \mathbf{D}^* \cdot \boldsymbol{\tau})]}_{\text{elastic}}. \tag{28}$$

This can be known as the informed viscoelastic (iVE) equation, which incorporating the shear and extension viscous contributions, as well as the elastic effects. When Wi equals zero, the WMT-X viscoelastic model returns to the GNF-X viscous model. According to the steady-state and homogenous stress tensor under simple shear flow, the shear stress τ_{12}, the first normal stress difference N_1 and the second normal stress difference N_2 are further found as below:

$$\tau_{12} = \frac{\eta_S\dot{\gamma}}{1 + \text{Wi}^2(1 - C_N^2)} \tag{29}$$

$$N_1 = \tau_{11} - \tau_{22} = 2\text{Wi}\tau_{12} \tag{30}$$

$$N_2 = \tau_{22} - \tau_{33} = -(1 - C_N)\text{Wi}\tau_{12} \tag{31}$$

$$-\frac{N_2}{N_1} = \frac{(1 - C_N)}{2} = \frac{\xi}{2} \tag{32}$$

$$C_N = 1 - 2\left(-\frac{N_2}{N_1}\right), \tag{33}$$

where τ_{11}, τ_{22}, and τ_{33} are the x-axial, y-axial, and z-axial normal stress tensor components, respectively; τ_{12} occurs in the xy plane.

During the shear flow, the Weissenberg number Wi has proven invaluable for rheologists in quantifying the viscoelastic effects in a non-Newtonian fluid, which is the product of the strain rate $\dot{\gamma}$ and the longest relaxation time λ_W:

$$\mathrm{Wi} = \lambda_W \dot{\gamma}. \tag{34}$$

At a large Weissenberg number, Wi >> 1, the fluid will respond with elastic behavior like that of a solid. For Wi << 1, a liquid-like viscous state is expected, while there is sufficient time to relax during deformation. One can assume the strain-rate dependence of $\mathrm{Wi}(\dot{\gamma})$ and $\lambda_W(\dot{\gamma})$. Thus, the relaxation time $\lambda_W(\dot{\gamma})$ is determined via Eq. (34):

$$\lambda_W(\dot{\gamma}) = \frac{\mathrm{Wi}(\dot{\gamma})}{\dot{\gamma}}. \tag{35}$$

For avoiding the high Weissenberg number problem [8] with unstable numerical calculations, one attempts to improve the unconstrained growth of Weissenberg function with respect to strain rates:

$$\mathrm{Wi}(\dot{\gamma}) = \frac{\mathrm{Wi}_0}{\left[1 + \left(\frac{\dot{\gamma}}{\dot{\gamma}_{CW}}\right)^{-2}\right]^{n_W}}, \tag{36}$$

where the parameters Wi_0, $\dot{\gamma}_{CW}$, and n_W are fit by the experimental data of the first normal stress difference. Thus, the unstable high Wi problem is weakened by such a constrained Weissenberg growth function. Details of the WMT-X model scheme are referred to in the previous work of Tseng [8].

In addition, the elastic variable C_N is related to the minus-normal-stress-difference ratio of $-N_2/N_1$ [see Eq. (33)]. The $(-N_2/N_1)$ ratio reasonably exists in a region between 0 and 0.5 for general polymer melts. Thus, the ratio is assumed the independence of temperature, and is modeled as a step function of strain rates:

$$\left(-\frac{N_2}{N_1}\right) = R_0 + \frac{0.5 - R_0}{\left[1 + \left(\frac{\dot{\gamma}}{\dot{\gamma}_{CR}}\right)^2\right]^{n_R}}, \tag{37}$$

where the parameters R_0, $\dot{\gamma}_{CR}$, and n_R are fit by the experimental data. When $-N_2/N_1 = 0$ and 0.5, the variable C_N equals one and zero, respectively.

From theory to practice, the significant constitutive models, GNF-X and WMT-X, were incorporated into commercial simulation software of plastic injection molding, Moldex3D. The state-of-the-art Moldex3D CFD (computational fluid dynamics) framework is developed by the three-dimensional finite volume method (3D-FVM) [29] to numerically solve the transient, non-isothermal governing equations of flow fields for complicated viscoelastic fluids of polymer melts. In addition, the advantage of 3D-FVM with robustness and efficiency is the ability to realize a nonlinear imbalanced flow phenomenon in complex channel geometries.

2.4 Derivation of normal stress differences in hybrid shear/extensional flow

Consider that a hybrid flow of the velocity gradient tensor $\nabla\mathbf{v}$ consists of simple shear and planar extension:

$$\nabla\mathbf{v} = \begin{bmatrix} -\dot{\varepsilon} & 0 & \dot{\gamma}_S \\ 0 & \dot{\varepsilon} & 0 \\ 0 & 0 & 0 \end{bmatrix}, \tag{38}$$

where the compression and stretch deformations are exerted along the x-axial and y-axial directions for the planar extension flow, respectively; the simple shear flow is given in the xz plane; $\dot{\varepsilon}$ and $\dot{\gamma}_S$ are the diagonal and off-diagonal components, respectively. Thereby, the rate-of-strain tensor $\mathbf{D}$ and total strain rate and the total strain rate $\dot{\gamma}$ are expressed as:

$$\mathbf{D} = \begin{bmatrix} -\dot{\varepsilon} & 0 & \frac{1}{2}\dot{\gamma}_S \\ 0 & \dot{\varepsilon} & 0 \\ \frac{1}{2}\dot{\gamma}_S & 0 & 0 \end{bmatrix} \tag{39}$$

$$\dot{\gamma}^2 = \sqrt{2\mathbf{D} : \mathbf{D}} = \dot{\gamma}_S^2 + \dot{\gamma}_E^2 \tag{40}$$

$$\dot{\gamma}_E = 2\dot{\varepsilon}, \tag{41}$$

where $\dot{\gamma}_S$ and $\dot{\gamma}_E$ are the characteristic shear and extensional rates, respectively.

According to the upper convected form of the WM model of Eq. (30), the first normal stress difference N_1^S (abbreviation: **N1S**) for the steady-state and homogenous simple shear flow is shown as:

$$N_1^S = \tau_{11} - \tau_{33} = 2\eta_S \dot{\gamma}_S \mathrm{Wi}, \tag{42}$$

where τ_{11}, τ_{22}, and τ_{33} are the x-axial, y-axial, and z-axial normal stress tensor components, respectively. In addition, the planar extensional viscosity is defined as:

$$\eta_{PE} = \frac{\tau_{22} - \tau_{11}}{\dot{\varepsilon}} = \frac{N_1^E}{\dot{\varepsilon}}, \tag{43}$$

where N_1^E (abbreviation: **N1E**) is the first normal stress difference due to the planar extension flow.

This is based on the Trouton ratio of Eq. (10):

$$N_1^E = \mathrm{Tr}\eta_S \dot{\varepsilon}. \tag{44}$$

Therefore, the total first normal stress difference N_1^T(abbreviation: **N1T**) for hybrid shear/extension flow is expressed as:

$$N_1^{\mathrm{T}} = N_1^{\mathrm{S}} + N_1^{\mathrm{E}} = \eta_{\mathrm{S}}\dot{\gamma}_{\mathrm{S}}\left(2\mathrm{Wi} + \frac{1}{2}\mathrm{Tr}\frac{\dot{\gamma}_{\mathrm{E}}}{\dot{\gamma}_{\mathrm{S}}}\right). \tag{45}$$

In dimensional forms, the stresses are written as follows:

$$\frac{N_1^{\mathrm{T}}}{\eta_{\mathrm{S}}\dot{\gamma}_{\mathrm{S}}} = 2\mathrm{Wi} + \frac{1}{2}\mathrm{Tr}\frac{\dot{\gamma}_{\mathrm{E}}}{\dot{\gamma}_{\mathrm{S}}} \tag{46}$$

$$\frac{N_1^{\mathrm{S}}}{\eta_{\mathrm{S}}\dot{\gamma}_{\mathrm{S}}} = 2\mathrm{Wi} \tag{47}$$

$$\frac{N_1^{\mathrm{E}}}{\eta_{\mathrm{S}}\dot{\gamma}_{\mathrm{S}}} = \frac{1}{2}\mathrm{Tr}\frac{\dot{\gamma}_{\mathrm{E}}}{\dot{\gamma}_{\mathrm{S}}}. \tag{48}$$

For the percentage of N_1^{E} and N_1^{S}, one can find:

$$\frac{N_1^{\mathrm{E}}}{N_1^{\mathrm{T}}} = \frac{1}{1 + 4(\mathrm{Wi}/\mathrm{Tr})(\dot{\gamma}_{\mathrm{S}}/\dot{\gamma}_{\mathrm{E}})} \tag{49}$$

$$\frac{N_1^{\mathrm{S}}}{N_1^{\mathrm{T}}} = 1 - \frac{N_1^{\mathrm{E}}}{N_1^{\mathrm{T}}}. \tag{50}$$

Thus, the $N_1^{\mathrm{S}}/N_1^{\mathrm{E}}$ ratio is expressed as:

$$\frac{N_1^{\mathrm{S}}}{N_1^{\mathrm{E}}} = 4\frac{\mathrm{Wi}}{\mathrm{Tr}}\frac{\dot{\gamma}_{\mathrm{S}}}{\dot{\gamma}_{\mathrm{E}}}. \tag{51}$$

From the GNF-X model of Eq. (16), the $\dot{\gamma}_{\mathrm{S}}/\dot{\gamma}_{\mathrm{E}}$ ratio is related to the weighted function W of extension fraction:

$$\frac{\dot{\gamma}_{\mathrm{S}}}{\dot{\gamma}_{\mathrm{E}}} = \sqrt{\frac{1-W}{W}}. \tag{52}$$

In the next section, dramatic variations of the stresses, N_1^{E} and N_1^{S}, with respect to strain rates are investigated in analytical flows of hybrid simple shear/planar extension.

3 Results and discussion

In the present study, the main objective is to demonstrate the conflicting effects in the shear-induced and extension-induced first normal stress difference, N_1^{E} and N_1^{S}, which are related to the Trouton ratio and the Weissenberg number, respectively. For the analytical center-gated disk flow of power-law fluid, the primary necessity is to understand the characteristic shear rate and extension rate profiles, as well as the N_1^{E} and N_1^{S} distributions through the normalized thickness at various Weissenberg's numbers under the fixed higher Trouton ratio. In addition to identifying the WMT-X parameters of material functions for LDPE melt, dramatic changes in N_1^{E} and N_1^{S} with respect to strain rates are investigated herein. As validation for different constitutive equations, including NF, GNF, GNF-X, and WMT-X, the slit velocity profile in contraction flow simulations are performed to explore if the inelastic extensional-viscosity-generating first normal stress difference N_1^{E} can obviously increase flow resistance, whereas the elastic shear-induced first normal stress difference N_1^{S} can have the opposite effect to facilitate flow momentum.

3.1 Analytical center-gated disk flow of power-law fluid

The center-gated disk flow of the velocity gradient tensor is guided by a complex combination flow consisting of the off-diagonal shear component and diagonal extension component, as shown in Fig. 1. For the power-law fluid, the analytical velocity gradient tensor $\mathbf{L}$ of the center-gated disk is given to determine the symmetric rate-of-deformation tensor $\mathbf{D}$ and the anti-symmetric vorticity tensor $\mathbf{W}$:

$$\eta = \eta_0\dot{\gamma}^{n-1} \tag{53}$$

$$s = 1/n \tag{54}$$

$$v_{\mathrm{r}} = \frac{Q}{4\pi rb}\left(\frac{s+2}{s+1}\right)\left[1 - \left(\frac{z}{b}\right)^{s+1}\right], \quad v_\theta = 0, \quad v_z = 0 \tag{55}$$

$$\mathbf{L} = \nabla\mathbf{v} = \frac{Q}{4\pi rh}\left(\frac{s+2}{s+1}\right)\begin{bmatrix} -\frac{1}{r}\left[1 - \left(\frac{z}{h}\right)^{s+1}\right] & 0 & -\frac{s+1}{h}\left(\frac{z}{h}\right)^{s} \\ 0 & \frac{1}{r}\left[1 - \left(\frac{z}{h}\right)^{s+1}\right] & 0 \\ 0 & 0 & 0 \end{bmatrix} \tag{56}$$

$$= \begin{bmatrix} -L_{\mathrm{E}} & 0 & L_{\mathrm{S}} \\ 0 & L_{\mathrm{E}} & 0 \\ 0 & 0 & 0 \end{bmatrix} \tag{57}$$

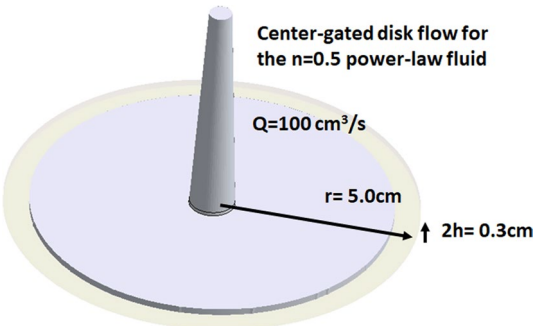

Fig. 1 Illustration of the center-gated disk flow for the $n = 0.5$ power-law fluid

$$L_{\mathrm{S}} = \frac{Q}{4\pi}\frac{1}{r}\frac{s+2}{h^2}\left(\frac{z}{h}\right)^{s} \tag{58}$$

$$L_{\mathrm{E}} = \frac{Q}{4\pi}\frac{1}{r^2}\frac{1}{h}\left(\frac{s+2}{s+1}\right)\left[1-\left(\frac{z}{h}\right)^{s+1}\right], \tag{59}$$

where Q is the volumetric flow rate; the total gap thickness is $2h$; v_i is the velocity component in the x_i direction, with the subscripts $i,j = r,\theta,z$ in the cylindrical coordinates; $0 < r \le R$ is constrained, and R is the disk radius. By using the cylindrical coordinates, the radial distance r describes the flow direction: the azimuth angle θ is in the cross-flow direction, and the z axis is in the gradient direction. The velocity gradient tensor component is defined as:$L_{ij} = \partial v_i/\partial x_j$. L_{S} and L_{E} are the shear and extension components of the velocity gradient tensor, respectively.

The rate-of-strain tensor $\mathbf{D}$ and total strain rate $\dot{\gamma}$ depending on L_{S} and L_{E} are obtained, as well:

$$\mathbf{D} = \begin{bmatrix} -L_{\mathrm{E}} & 0 & \frac{L_{\mathrm{S}}}{2} \\ 0 & L_{\mathrm{E}} & 0 \\ \frac{L_{\mathrm{S}}}{2} & 0 & 0 \end{bmatrix} \tag{60}$$

$$\dot{\gamma}^2 = \sqrt{2\mathbf{D} : \mathbf{D}} = L_{\mathrm{S}}^2 + (2L_{\mathrm{E}})^2 \tag{61}$$

The characteristic shear and extension rates, $\dot{\gamma}_{\mathrm{S}}$ and $\dot{\gamma}_{\mathrm{E}}$, can both be discriminated:

$$\dot{\gamma}_{\mathrm{S}} = L_{\mathrm{S}} \tag{62}$$

$$\dot{\gamma}_{\mathrm{E}} = 2L_{\mathrm{E}} \tag{63}$$

$$\dot{\gamma}^2 = \dot{\gamma}_{\mathrm{S}}^2 + \dot{\gamma}_{\mathrm{E}}^2. \tag{64}$$

In this work, the disk thickness and disk radius are $2h = 0.3$ cm and $r = 5.0$ cm; the flow rate $Q = 100$ cm^3/s is given. For the power-law fluid with the power index $n = 0.5$, Fig. 2 shows total strain rate, shear rate, and extension rate profiles through the normalized thickness in analytical isothermal center-gated disk flow. Shear rate is the largest proportion of total strain rate. The maximum shear rate $\dot{\gamma}_{\mathrm{S}}^{\max} = 212.2\ \mathrm{s}^{-1}$ obviously occurs in the wall boundary ($z/h = 1.0$), while the zero-shear-rate is found at the flow center ($z/h = 0.0$). Conversely, the maximum extension rate $\dot{\gamma}_{\mathrm{E}}^{\max} = 5.6\ \mathrm{s}^{-1}$ is limited in the center and is close to zero near the wall. In Fig. 3, the extension fraction profile clearly concentrates at the thickness core. As shown in Fig. 4, one can attempt to find the relationship between extension fraction and strain rates. Thereby, the extension fraction or weighted function of the GNF-X model is expressed below:

$$W = \frac{\dot{\gamma}_{\mathrm{E}}^2}{\dot{\gamma}^2} = \frac{1}{\left[1+\left(\frac{\dot{\gamma}}{\dot{\gamma}_{\mathrm{C}}}\right)\right]^{N_{\mathrm{W}}}}, \tag{65}$$

where the critical strain rate is $\dot{\gamma}_{\mathrm{C}} = 10\ \mathrm{s}^{-1}$; the power index is $N_{\mathrm{W}} = 1.3$.

The $\dot{\gamma}_{\mathrm{S}}/\dot{\gamma}_{\mathrm{E}}$ ratio is estimated based on Fig. 4 of the extension fraction. In particular, $\mathrm{Wi} = 0$ is given in the preceding Eqs. (49) and (50) so that $\frac{N_1^{\mathrm{E}}}{N_1^{\mathrm{T}}} = 1$ and $\frac{N_1^{\mathrm{S}}}{N_1^{\mathrm{T}}} = 0$ are obtained for inelastic power-law fluids with the power index $n = 0.5$. At various Weissenberg's numbers ($\mathrm{Wi} = 0.1$, 1.0, and 10) under the fixed higher Trouton ratio of $\mathrm{Tr} = 30$, Fig. 5 shows the percentage of N_1^{E} and N_1^{S} through the normalized thickness from the center core to the wall boundary. Exhibiting the opposite relation

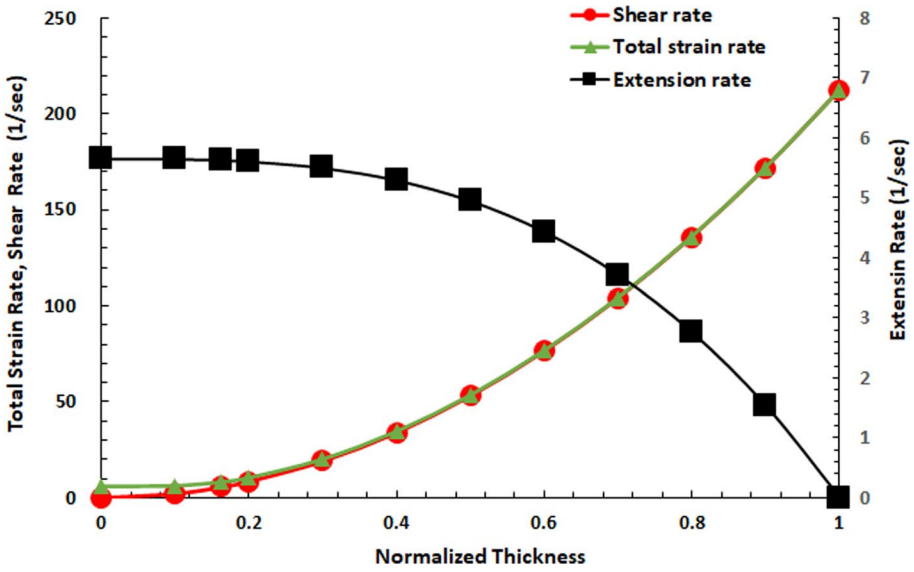

Fig. 2 Total strain rate, shear rate, and extension rate profiles through the normalized thickness for the analytical center-gated disk flow of isothermal power-law fluid ($n = 0.5$)

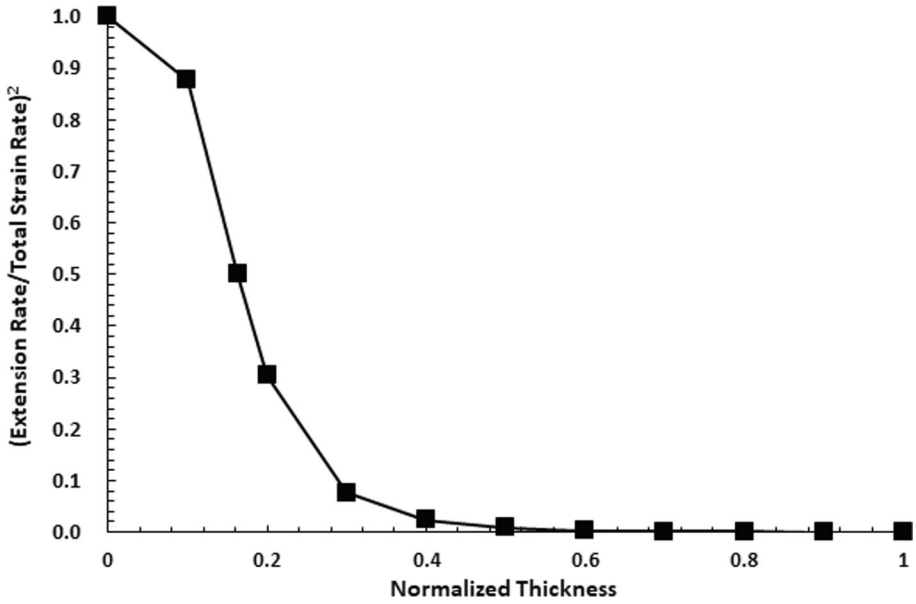

Fig. 3 Extension fraction profiles through the normalized thickness for the analytical center-gated disk flow of isothermal power-law fluid ($n=0.5$)

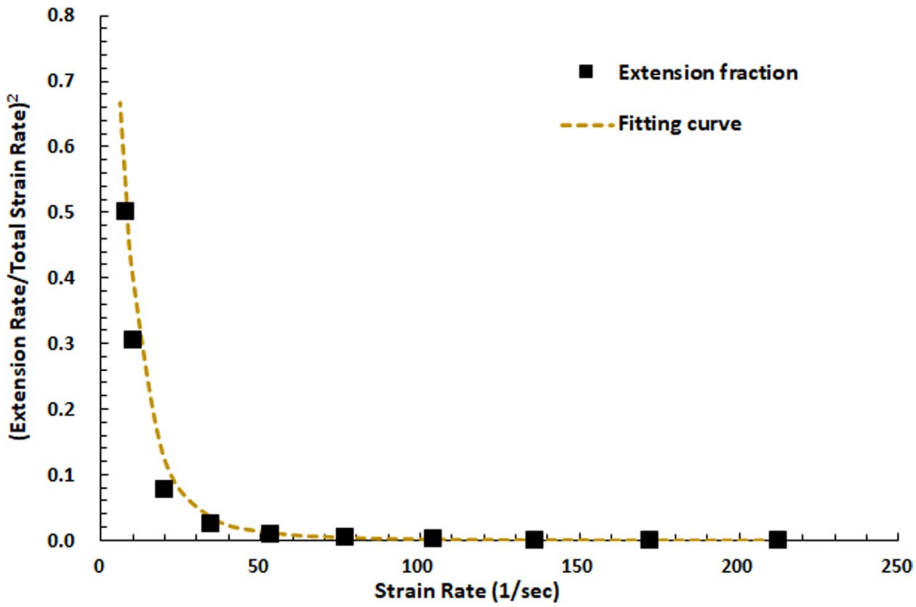

Fig. 4 Extension fraction against strain rates for the analytical center-gated disk flow of isothermal power-law fluid ($n=0.5$)

between the inelastic extensional-viscosity-generating first normal stress difference N_1^E and the elastic shear-induced first normal stress difference N_1^S is obvious. In addition, N_1^E occurs at the core and N_1^S yields near the boundary. For the weak elastic effect with the small Weissenberg number of $Wi=0.1$, N_1^E almost dominates 90% of whole region, while N_1^S occupies about 10%. Increasing the elastic effect at $Wi=1.0$, N_1^E and N_1^S control 40% and 60%, respectively. In particular, due to the strong elastic effect with the extreme value of $Wi=10$, it conversely results in 10% of N_1^E and 90% of N_1^S. Therefore, higher N_1^E corresponds to lower N_1^S, and vice versa. When the Weissenberg number of elastic effect is increased, the elastic shear-induced first normal stress difference N_1^S becomes stronger, but the inelastic extensional-viscosity-generating first normal stress difference N_1^E is weak. Such a result verifies the conflicting role of N_1^E and N_1^S with respect to Weissenberg numbers in the analytical center-gated disk flow for the non-Newtonian fluid of power-law model.

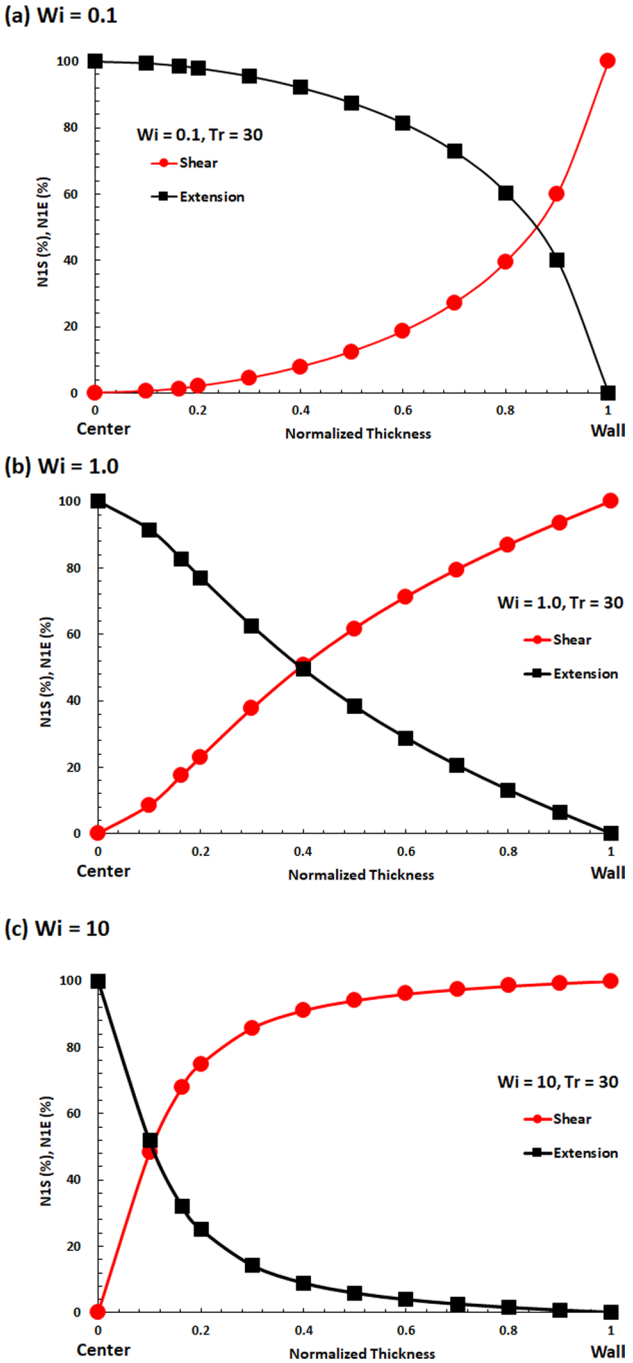

Fig. 5 Percentage of N1S and N1E profiles through the normalized thickness at various Weissenberg's numbers for the analytical center-gated disk flow of isothermal power-law fluid ($n = 0.5$)

3.2 Variations of N1S and N1E with respect to strain rates

Referring to the previous work of Mitsoulis et al. [30], experimental rheological data on LDPE (low-density polyethylene) melt at the isothermal temperature of 150 °C contain the shear viscosity, the extensional viscosity, and the first normal stress normal difference N_1. The WMT-X viscoelastic constitutive Eq. (24) incorporates the Carreau model of shear viscosity of Eq. (9) and the Trouton ratio model of extensional viscosity of Eq. (12), as well as the Weissenberg function of the first normal stress difference of Eq. (36) and the $(-N_2/N_1)$ ratio of Eq. (37). Figures 6 and 7 show all material functions, including the shear viscosity, the extensional viscosity, and the first normal stress difference, with respect to strain rates. The predictive curves match the related experimental data. Figure 8 presents the Trouton ratio, the Weissenberg function, and the $(-N_2/N_1)$ ratio. All optimal model parameters are addressed in Table 1. The identified WMT-X parameters are used in the next section for the contraction flow simulations.

Following the preceding result of the extension fraction with respect to strain rates in Fig. 4 for the hybrid simple shear/planar extension flow, Fig. 9 shows the shear-induced first normal stress difference N_1^S and the extensional-viscosity-generating inelastic first normal stress difference N_1^E against strain rates $\dot{\gamma}$ in dimensionless units, as well as the total first normal stress difference N_1^T. A critical strain rate is found: $\dot{\gamma}'_C = 50\ s^{-1}$; the critical strain rate is influenced by the Weissenberg number and the Trouton ratio. Obviously, N_1^S dominates at high strain rates of $\dot{\gamma} > \dot{\gamma}_C$, whereas N_1^E occurs at low strain rates of $\dot{\gamma} < \dot{\gamma}_C$. In addition, N_1^E is larger than N_1^S. Furthermore, Fig. 10 presents the N_1^S/N_1^E ratio to reveal N_1^S and N_1^E at the high and low strain rates, respectively. The competing roles of N_1^S and N_1^E percentage distributions with respect to strain rates in Fig. 11 are clearly indicated as well.

3.3 Slit velocity profile in contraction flow simulation

Following the same used material of 150 °C LDPE melt aforementioned, the experimental data of Schmidt et al. [31] regarding the slit velocity profile within a inhomogenous 14:1 planar contraction flow were of interest herein. The primary objective is to demonstrate N_1^S facilitating flow and N_1^E hindering flow for the velocity profile. Figure 12 illustrates the half symmetric geometry of 14:1 planar contraction flow, which includes two parts: the upstream channel of fluid reservoir and the downstream channel of slit die. The square cross section of the reservoir is $14 \times 14\ mm^2$ and its length is 100 mm. The contraction ratio is 14 wherein the height of the reservoir and die is 14 and 1 mm, respectively. The die length is 50 mm. The apparent shear rate of $227\ s^{-1}$ (or flow rate of about $300\ mm^3/s$) is given for the slit die. Figure 13 shows the trustworthy experimental velocity profile within the slit die measured by Schmidt et al. [31]. They ensured the homogenous temperature distribution in the measurements and avoided some problems of flow instability and wall slip. The velocity profile presents a typical plug-like

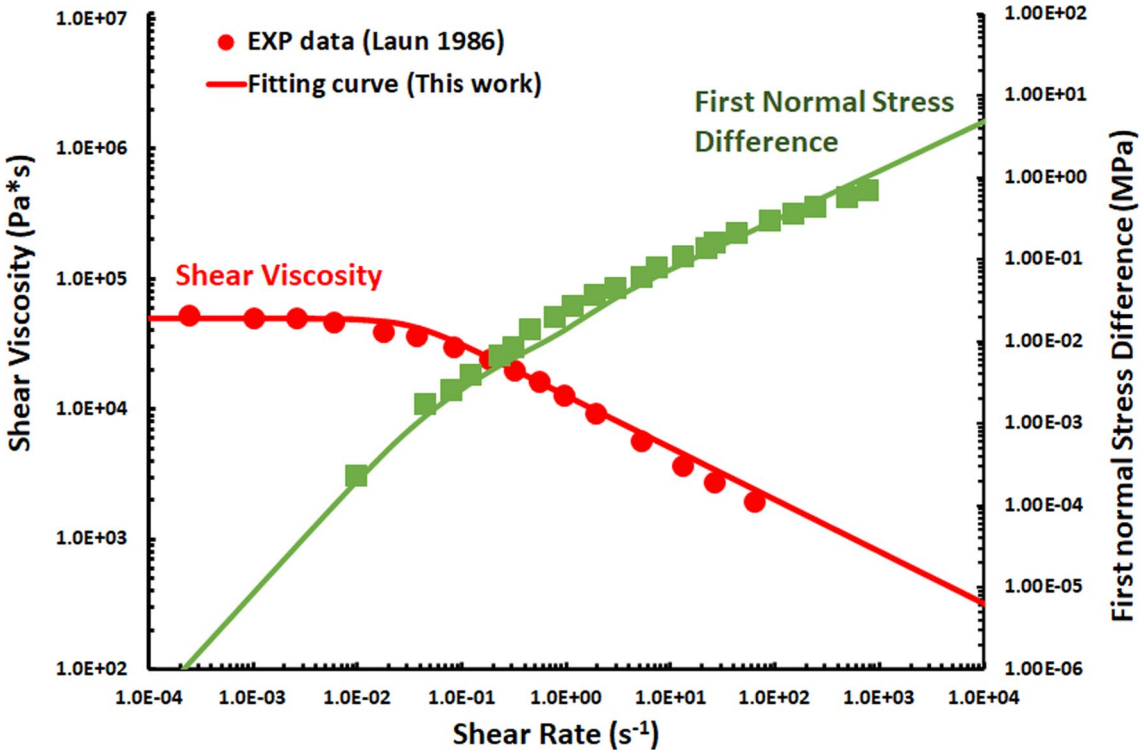

Fig. 6 Shear viscosity and first normal stress difference against shear rates for molten LDPE at 150 °C; solid symbols and solid lines represent experimental data and fitting curves, respectively

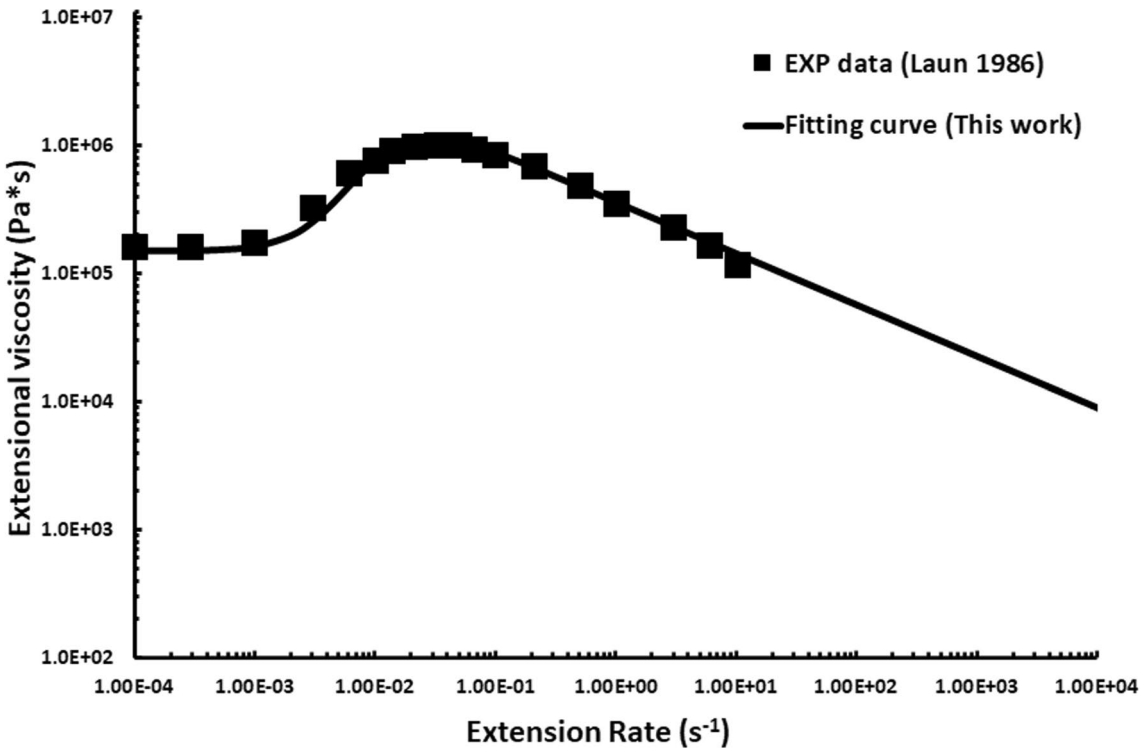

Fig. 7 Uniaxial extensional viscosity against extension rates for molten LDPE at 150 °C; solid symbols and solid lines represent experimental data and fitting curves, respectively

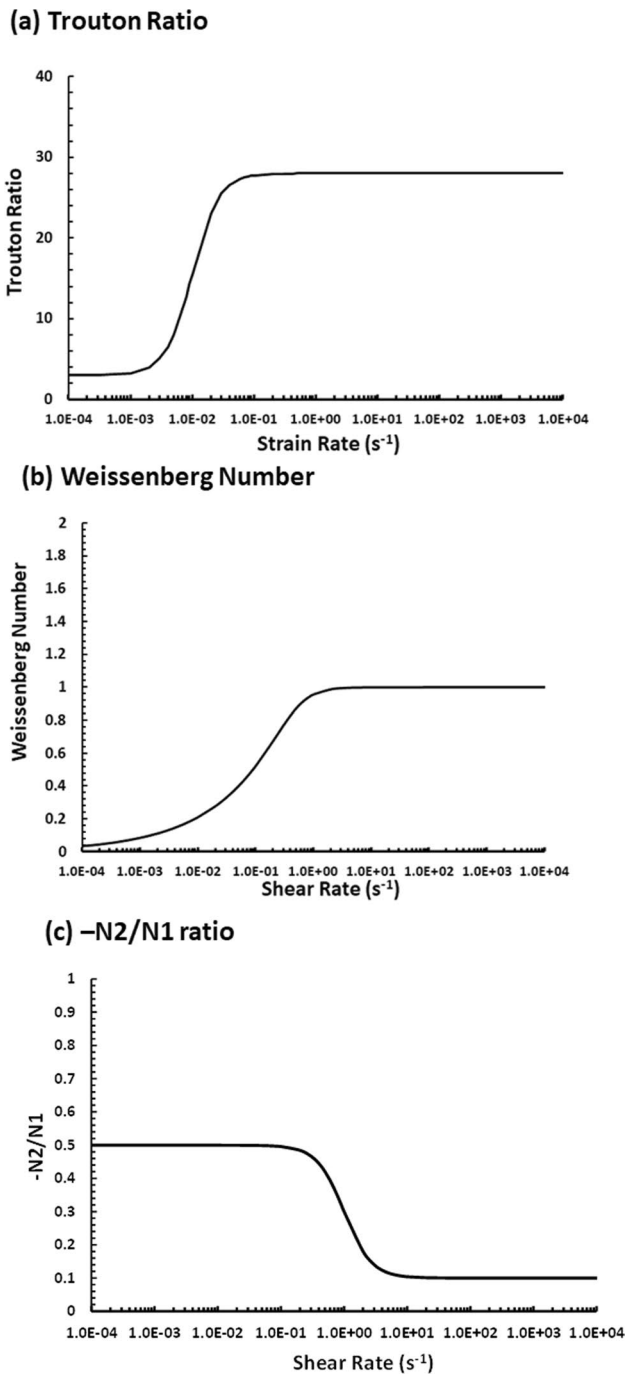

Fig. 8 Trouton ratio, Weissenberg number, and $-N_2/N_1$ ratio against strain rates for molten LDPE at 150 °C

shape; this result realistically confirms the general understanding of the theoretical analysis in rheology.

Referring to the previous work of Schmidt et al. [31], a research version of the commercial injection molding simulation software, Moldex3D (CoreTech System Co., Taiwan) was adopted to perform the contraction flow simulation in the present work. The number of 3D cells is about 1,000,000 hexagonal elements used in the flow computation for the contraction geometry in Fig. 12. The Cartesian coordinate system was defined in the description and analysis of the velocity fields. The identified viscous and viscoelastic parameters of the NF, GNF, GNF-X, and WMT-X models are addressed in Table 1.

Table 1 Model parameters of material functions for LDPE melt at 150 °C

Material functions	Model parameters	Value
Carreau model for shear viscosity	η_0 (Pa*s)	$5.0*10^4$
	λ (s)	30.0
	n	0.58
Trouton ratio for extensional viscosity	T_0	25.0
	λ_T (s)	100.0
	n_T	1.0
Weissenberg number for N_1	W_0	1.0
	$\dot{\gamma}_{CW}$ (s^{-1})	0.5
	n_W	0.25
WMT-X model for $-N_2/N_1$	R_0	0.1
	$\dot{\gamma}_{CR}$ (s^{-1})	1.0
	n_R	1.0

The early studies indicated that the temperature increase leads to opposite variations of the viscosity [32]. For high shear rates, shear heating viscous dissipation will increase substantially the downstream slit-wall temperature in the contraction flow. Typically, note that a pressure drop of 10 MPa will induce a temperature increase of around 2 °C. At a high shear rate of 10,000 s^{-1} and a high pressure drop of 100 MPa, the mean temperature rise could be as high as 20 °C which will influence the viscosity. In the present study, such a slit-contraction flow simulation was performed by the Moldex3D software kept at the *isothermal* temperature of $T = 150$ °C at the lower appear shear rate of 227 s^{-1}. Recently, Wen et al. [18] performed the *non-isothermal* GNF-X flow simulations to estimate the extensional viscosity for various polymer melts.

As a result, the predictions of velocity profiles for different constitutive models of viscous and viscoelastic fluids are shown in Fig. 13. For the linear NF constant viscosity and the nonlinear GNF shear viscosity, the predicted velocity profile clearly presents the parabolic curve with over-estimation as compared with the experimental date. Basically, the nonlinear GNF shear viscosity increases the flow resistance. In addition, the GNF-X model results in the plug-flow distribution with under-prediction. Obviously, the central velocity slows down due to the resistance contribution of extensional viscosity. It is significant that the predictive curve by the WMT-X viscoelastic model is close to the experimental

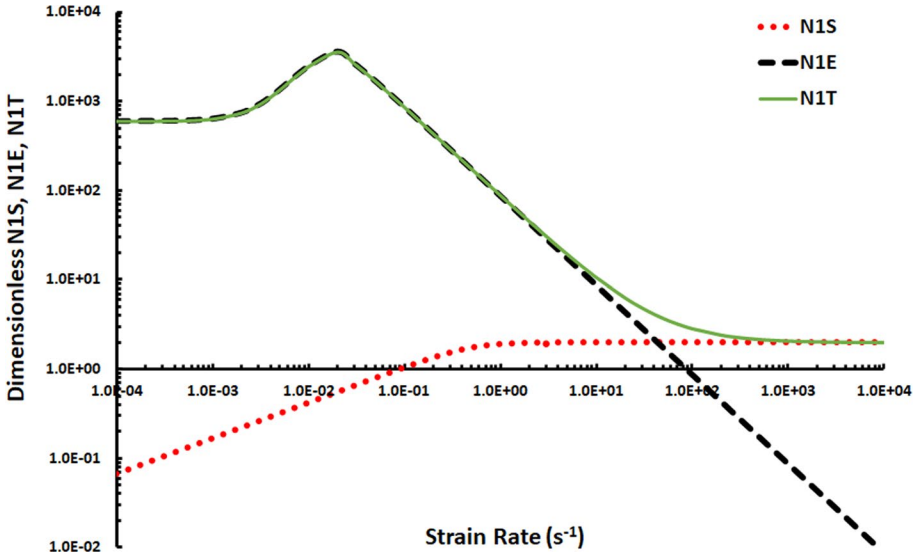

Fig. 9 Dimensionless N1S, N1E, N1T against strain rates for molten LDPE at 150 °C

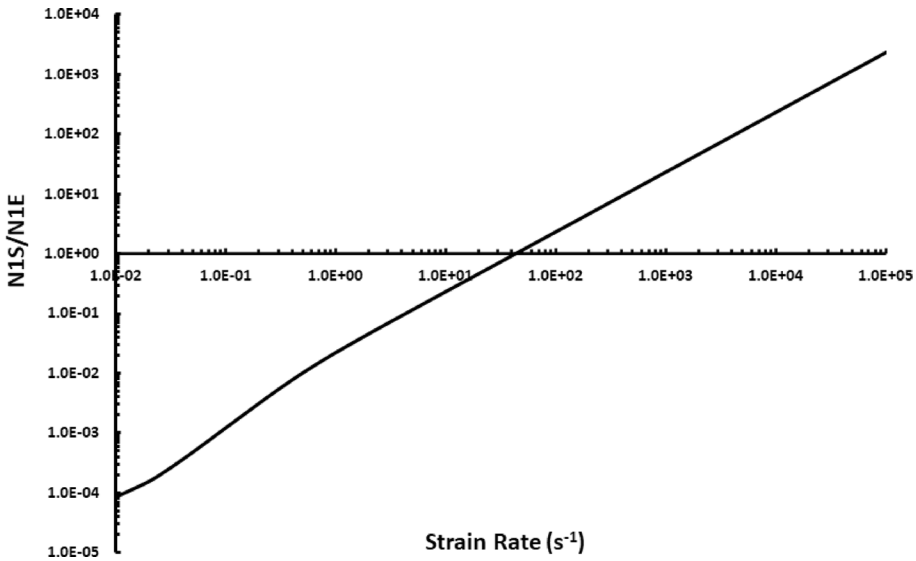

Fig. 10 The ratio of N1S to N1E against strain rates for molten LDPE at 150 °C

data of Schmidt et al. [31]. Therefore, one can focus the whole velocity profile especially for GNF-X and WMT-X models, confirming the importance of the elastic effect of the first normal stress difference to accelerate the flowing speed, whereas the GNF-X model with extensional viscosity provides the attaining of a flowing resistance. Previously, the WMT-X viscoelastic model was used to find the vertex growth phenomenon [6, 8], which was slightly affected by the elastic effect of the first normal stress difference. Notably, the inelastic extensional-viscosity-generating first normal stress difference N_1^E hinders flow, whereas the elastic shear-induced first normal stress difference N_1^S can have the opposite effect in facilitating the flow. Therefore, it evidently demonstrates the opposite effect of the normal stresses N_1^S and N_1^E for the slit velocity in the contraction flow of LDPE melt.

In particular, a comparison of extensional-thickening and extensional-thinning viscosity curves at low

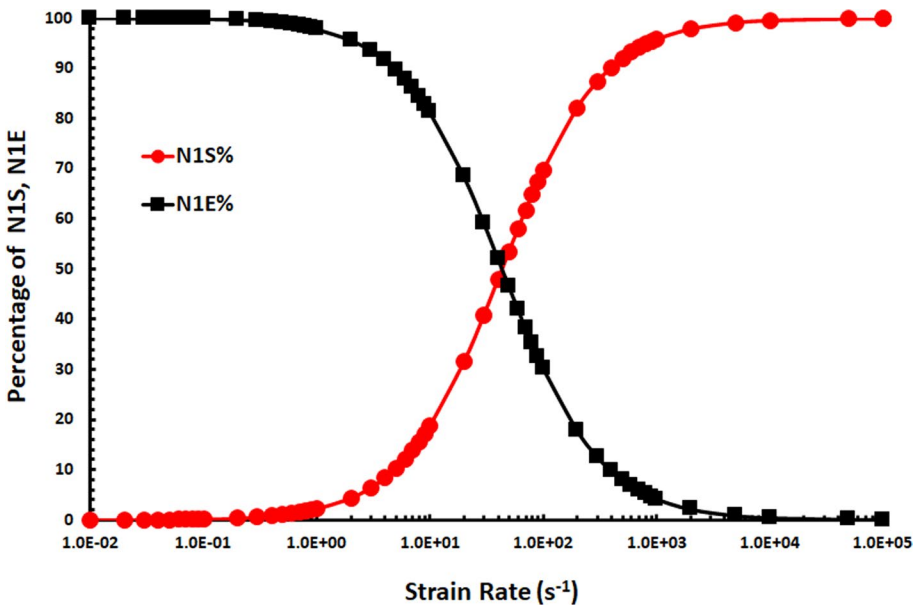

Fig. 11 The percentage of N1S and N1E against strain rates for molten LDPE at 150 °C

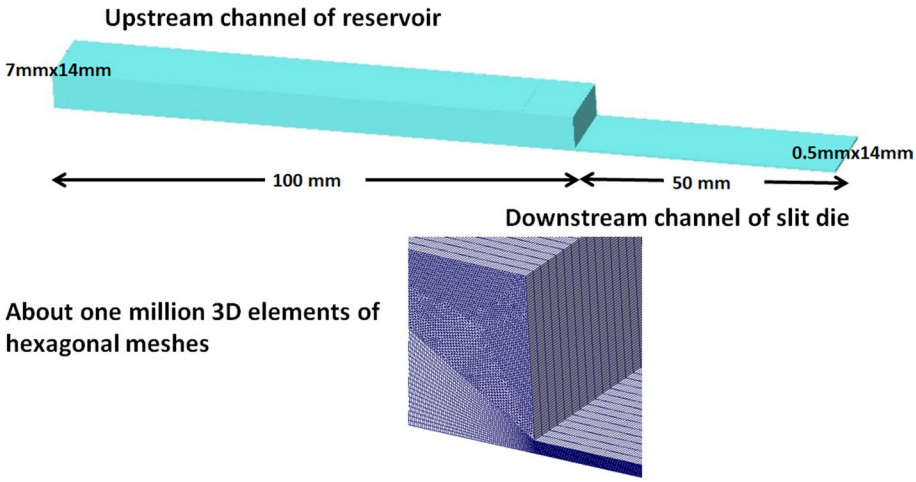

Fig. 12 The half symmetric geometry of 14:1 planar contraction flow with slit die

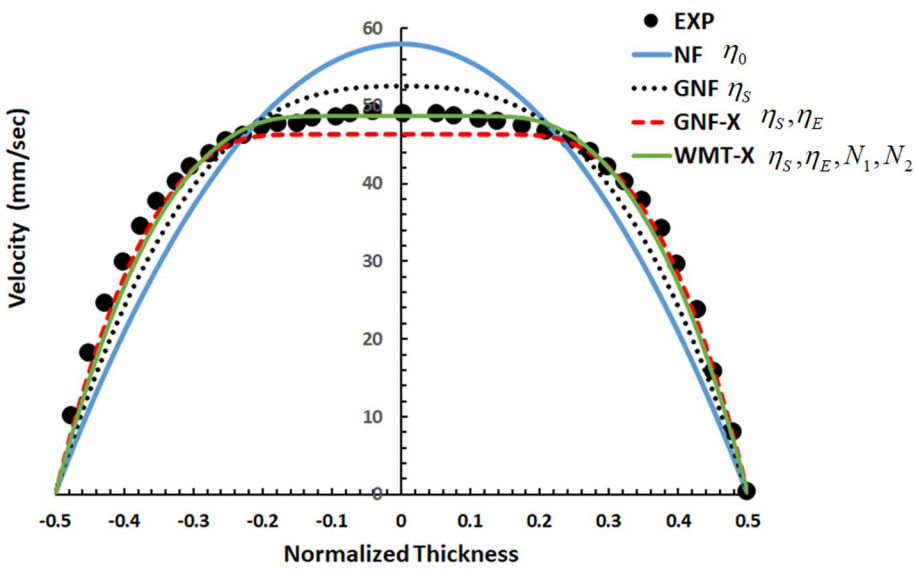

Fig. 13 Velocity profiles within the die slit for the LDPE melt at 150 °C and 227 s^{-1} for differential viscous and viscoelastic constitutive models

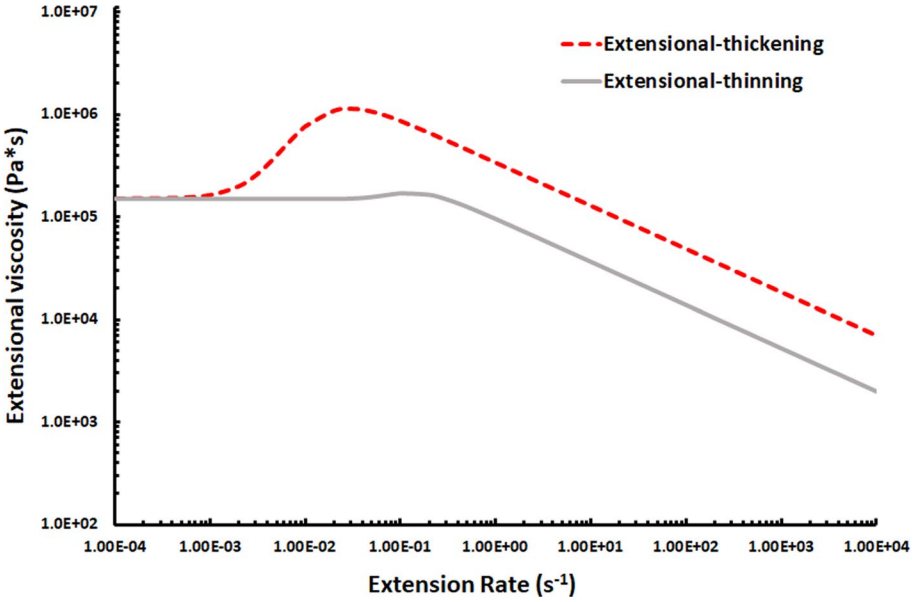

Fig. 14 Extensional viscosity curves for extensional-thickening and extensional-thinning

Table 2 Trouton ratio for extensional-thickening and extensional-thinning

Model parameters	Extensional-thickening	Extensional-thinning
T_0	25.0	5.0
λ_T (s)	100.0	10.0
n_T	1.0	1.0

extension rates shown in Fig. 14.The extensional viscosity model parameters of Trouton ratio are addressed in Table 2. Thereby, Fig. 15 presents that the central velocity of the extensional-thinning fluid is faster than that of the extensional-thinning fluid. It is evident to explore the difference between extensional-thinning and extensional-thinning.

4 Conclusions

Using the WMT-X viscoelastic model, the ultimate goal was to demonstrate the conflicting roles of the inelastic extensional viscosity-generating first normal stress difference

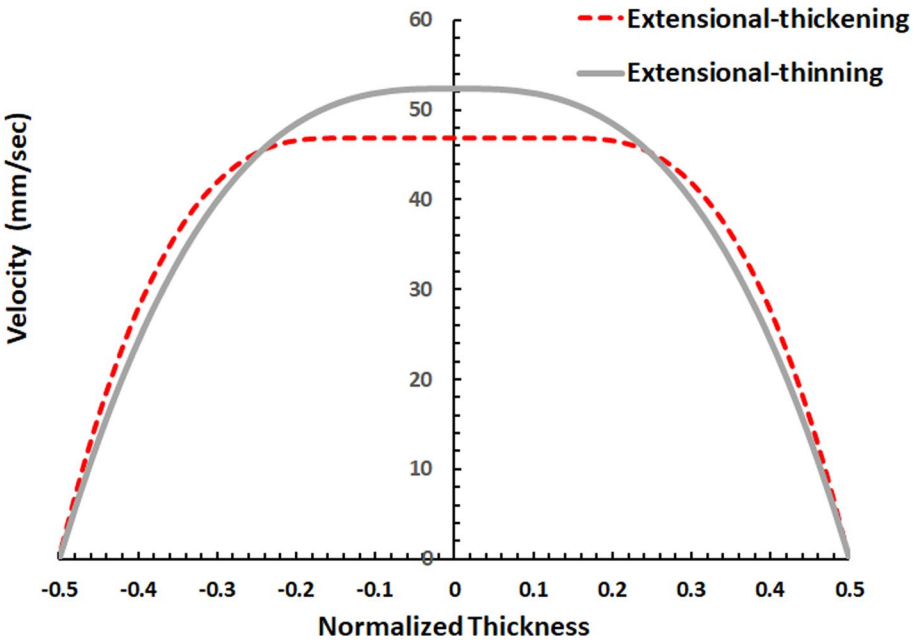

Fig. 15 Velocity profiles for extensional-thickening and extensional-thinning

N_1^E and the elastic shear-induced first normal stress difference N_1^S in hybrid shear/extension flow. As a whole. N_1^E is larger than N_1^S. Although N_1^S is somewhat small, it cannot be ignored. In addition, N_1^S and N_1^E dominate at high and low strain rates, respectively. When the Weissenberg number of elastic effect is increased, N_1^S becomes stronger, while N_1^E is relatively weak. For predicting the slit velocity profile in contractions flow simulations, it is significant to show N_1^S facilitating flow, albeit N_1^E has the opposite effect in hampering flow. In particular, it is evident to explore that the central velocity of the extensional-thinning fluid is faster than that of the extensional-thinning fluid.

Data availability Data will be made available on request.

Declarations

Conflict of interest The authors declare that they have no known competing financial interests or personal relationships that could have appeared to influence the work reported in this paper.

References

1. Debbaut B, Crochet MJ (1988) Extensional effects in complex flows. J Non-Newtonian Fluid Mech 30:169–184
2. Walters K, Tamaddon-Jahromi HR, Webster MF, Tomé MF, McKee S (2009) The competing roles of extensional viscosity and normal stress differences in complex flows of elastic liquids. Korea Aust Rheol J 21:225–233
3. James DF (2016) N 1 stresses in extensional flows. J Non-Newtonian Fluid Mech 232:33–42
4. Bird RB, Armstrong RC, Hassager O (1987) Dynamics of polymeric liquids: fluid mechanics, 2nd edn. Wiley-Interscience, New York
5. Tanner RI (1989) Engineering rheology. Oxford University Press, New York
6. Tseng H-C (2020) A revisitation of generalized newtonian fluids. J Rheol 64:493–504
7. White JL, Metzner AB (1963) Development of constitutive equations for polymeric melts and solutions. J Appl Polym Sci 7:867–1889
8. Tseng H-C (2021) A revisitation of white-metzner viscoelastic fluids. Phys Fluids 33:057115
9. Tseng H-C (2021) A constitutive analysis of stress overshoot for entangled polymers under start-up shear flow. Phys Fluids 33:051706
10. Tseng H-C (2021) A constitutive equation for fiber suspensions in viscoelastic media. Phys Fluids 33:071702
11. Macosko CW (1994) Rheology: principles, measurements, and applications. Wiley-VCH, New York
12. Morrison FA (2001) Understanding rheology. Oxford University, New York
13. Zheng R, Tanner RI, Fan X-J (2011) Injection molding: integration of theory and modeling methods. Springer, Berlin
14. Petrie CJS (2006) Extensional viscosity: a critical discussion. J Non-Newtonian Fluid Mech 137:15–23
15. Sarkar D, Gupta M (2001) Further investigation of the effect of elongational viscosity on entrance flow. J Reinf Plast Compos 20:1473–1484
16. Park JM (2020) Comment on "a revisitation of generalized newtonian fluids." J Rheol 64:1497
17. Tseng H-C (2023) Numerical visualization of extensional flows in injection molding of polymer melts. Int Polym Process 38:175–182
18. Wen Y-H, Wang C-C, Cyue G-S, Kuo R-H, Hsu C-H, Chang R-Y (2023) Extensional rheology of linear and branched polymer melts in fast converging flows. Rheol Acta 62:183–204
19. Schunk PR, Scriven LE (1990) Constitutive equation for modeling mixed extension and shear in polymer solution processing. J Rheol 1085–1119:34
20. Astarita G (1979) Objective and generally applicable criteria for flow classification. J Non-Newtonian Fluid Mech 6:69–76
21. Souza Mendes PR, Padmanabhan M, Scriven LE, Macosko CW (1995) Inelastic constitutive equations for complex flows. Rheol Acta 34:209–214
22. Thompson RL, de Souza Mendes PR (2011) A constitutive model for non-Newtonian materials based on the persistence-of-straining tensor. Meccanica 46:1035–1045
23. Thompson RL, de Souza Mendes PR, Naccache MF (1999) A new constitutive equation and its performance in contraction flows. J Non-Newtonian Fluid Mech 86:375–388
24. Brunn PO, Ryssel E (1997) The **ω-d** fluid: General theory with special emphasis on stationary two dimensional flows. Continuum Mech Thermodyn 9:73–82
25. Ryssel E, Brunn PO (1999) Flow of a quasi-newtonian fluid through a planar contraction. J Non-Newtonian Fluid Mech 85:11–27
26. Meissner J, Stephenson SE, Demarmels A, Portman P (1982) Multiaxial elongational flows of polymer melts—classification and experimental realization. J Non-Newtonian Fluid Mech 11:221–237
27. Bach A (2003) Extensional viscosity for polymer melts measured in the filament stretching rheometer. J Rheol 47:429
28. Cogswell FN (1972) Converging flow of polymer melts in extrusion dies. Polym Eng Sci 12:64–73
29. Chang R-Y, Yang W-H (2001) Numerical simulation of mold filling in injection molding using a three-dimensional finite volume approach. Int J Numer Methods Fluids 37:125–148
30. Mitsoulis E, Schwetz M, Münstedt H (2003) Entry flow of lDPE melts in a planar contraction. J Non-Newtonian Fluid Mech 111:41–61
31. Schmidt M, Wassner E, Münstedt H (1999) Setup and test of a laser doppler velocimeter for investigations of flow behaviour of polymer melts. Mech Time-Depend Mater 3:371–393
32. Agassant JF, Avenas P, Carreau PJ, Vergnes B, Vincent M (2017) Polymer processing 2e: principles and modeling. Hanser Publishers, Munich